Research Article
Geochemistry, Geophysics, Geosystems
DOI 10.1002/2016GC006548

Reconstruction of rocks petrophysical properties as input data for reservoir modeling

B. Cantucci[1], G. Montegrossi[2], F. Lucci[3], and F. Quattrocchi[1]

[1]Istituto Nazionale di Geofisica e Vulcanologia, Via Vigna Murata 605, 00141 Roma, Italy.

[2]CNR - IGG, Via G. La Pira 4, 50121 Firenze, Italy.

[3] Dip. Scienze – Università degli Studi Roma Tre, Largo S.L. Murialdo 1, 00146 Roma, Italy.

Corresponding author: Barbara Cantucci (barbara.cantucci@ingv.it)

Key Points:

- Reconstruction of heat capacity, thermal conductivity, permeability and porosity, integrating well log information and numerical modelling.
- Results show that the proposed method is valid and can be applied in other areas.
- Petrophysical data may be used as main input data for reservoir modelling during pre-feasibility studies.

This article has been accepted for publication and undergone full peer review but has not been through the copyediting, typesetting, pagination and proofreading process which may lead to differences between this version and the Version of Record. Please cite this article as doi: 10.1002/2016GC006548

Received: Jul 22, 2016; Revised: Oct 06, 2016; Accepted: Oct 24, 2016

Abstract

The worldwide increasing energy demand triggered studies focused on defining the underground energy potential even in areas previously discharged or neglected. Nowadays, geological gas storage (CO_2 and/or CH_4) and geothermal energy are considered strategic for low-carbon energy development.

A widespread and safe application of these technologies needs an accurate characterization of the underground, in terms of geology, hydrogeology, geochemistry and geomechanics. However, during pre-feasibility study-stage, the limited number of available direct measurements of reservoirs, and the high costs of reopening closed deep wells must be taken into account.

The aim of this work is try to overcome these limits, proposing a new methodology to reconstruct vertical profiles, from surface to reservoir base, of: *i)* thermal capacity, *ii)* thermal conductivity, *iii)* porosity and *iv)* permeability, through integration of well-log information, petrographic observations on inland outcropping samples and, flow and heat transport modelling.

As case study to test our procedure we selected a deep-structure, located in the medium Tyrrhenian Sea (Italy). Obtained results are consistent with measured data, confirming the validity of the proposed model.

Notwithstanding intrinsic limitations due to manual calibration of the model with measured data, this methodology represents a useful tool for reservoir and geochemical modellers that need to define petrophysical input data for underground modelling before the well reopening.

1 Introduction

The Intergovernmental Panel on Climate Change [*IPCC,* 2014] has recently outlined the essential role, among other technologies, of CO_2 geological storage and geothermal energy, to mitigate the effects of climate change and satisfy the worldwide increasing energy demand.

A widespread employment of these technologies requires a low-cost and rapid resource evaluation also in areas previously discharged or neglected because not considered economically favourable. In these areas, an accurate characterization of the potential reservoir in terms of geology, hydrogeology, geochemistry and geomechanics is a pre-requisite in order to optimize the available resources while minimizing the possible associated risks.

Several methodologies allow to estimate reservoir capacity and potentiality for energetic purposes, and among those, the most used methods are static and dynamic methods. Static approaches use algorithms, based on reservoir parameters as volume and porosity to evaluate the available pore space and the recoverable heat at regional scale; or more in general the class of "volume methods" perform a Monte Carlo sensitivity check on an exploitation function (e.g., heat recovery) based on reservoir properties [*Williams*, 2014]. Dynamic methods are based on both analytical and numerical modelling to predict the fluid and heat behaviour within the reservoir, over the time. In this framework, thermal and hydraulic properties of rocks constitute the key parameters to assess the storage capacity [*Bachu et al.,* 2007; *Goodman et al.,* 2011; *Blondes et al.,* 2013; *Cantucci et al.,* 2016] and the geothermal potential [*Nathenson,* 1975; *Muffler and Cataldi,* 1978; *Muffler*, 1979; *Williams*, 2014] of identified reservoirs, for both static and dynamic approaches.

Thermal capacity and thermal conductivity of rocks represent the capacity of material to accumulate and transfer heat, respectively. Their values are an intrinsic material property and strictly depend on mineral composition of rocks, fluid content, temperature and degree of

isotropy of the rock. These parameters are required in evaluating the regional heat flow, the heat transfer for investigating engineering solutions, and the potential of geothermal reservoirs.

Porosity and permeability are the key parameter controlling the fluid flow and the transport processes in porous media. Porosity is a measure of the pore space available to the fluids and is used to estimate e.g., potential storage volume for gas. Permeability is a rock property controlling the rate at which fluids can move inside the reservoir and allows an estimate of the ability to extract or inject fluids in/from the available volume.

Porosity, permeability and thermal properties of rocks strictly depend on the tectonic history and the evolution of a specific area and should be measured directly in the laboratory on core drilled rock samples or in situ thought accurate well testing. The ranges of these parameters given in compilations of rock properties [e.g., *Birch,* 1966; *Čermák and Rybach,* 1982; *Haenel et al.,* 1988; *Clauser and Huenges*, 1995; *Clauser*, 2006] are too wide to be useful to constrain properties at a specific site.

Unfortunately, during the pre-feasibility stage of a project, economic resources are limited, and the reopening of closed deep wells may be very expensive, precluding the possibility to obtain direct measurements. Moreover, information reported in public well logs, often report only stratigraphic and physical parameters measured during the drilling such as temperatures, pressures, mud-loss and, rarely, fluid chemistry of the geological formations.

This research aims at developing a procedure that allows to estimate petrophysical properties of the rock formations when no direct measures of thermal capacity, thermal conductivity, porosity and permeability are available.

The presented methodology employed well known indirect methods to define total thermal capacity and thermal conductivity of a rock formation as a function of thermal properties of all rock-forming mineral phases with respect to their abundances and their relative fabric as obtained by petrographic analyses [*Rosen and Hashin,* 1970; *Berryman,* 1995; *Clauser and Huengesn,* 1995; *Clauser, 2006*].

Afterward, the obtained thermal properties of rocks were expressed as a function of porosity assuming that: *i)* all pores were water-filled, and *ii)* increasing of porosity would modify proportionally both thermal capacity and thermal conductivity. On the basis of well-known porosity-permeability relationships, with a trial-and-error procedure, vertical profiles of porosity and permeability were reconstructed by simulations of heat and mass transport using well log measured temperatures as boundary condition. Numerical modelling was performed by means of SHEMAT software package [*Clauser*, 2003].

An offshore carbonatic reservoir located in central Italy, already identified as potential target for geological storage of gas (CO_2 and/or CH_4) [*Procesi et al.,* 2013; *Buttinelli et al.,* 2014; *Cantucci et al.,* 2015] was selected as case study to test this approach.

2 The case study area

The study area is constituted by a deep structure (about 1900 m b.s.l.) located offshore in the eastern side of the Tyrrhenian Sea back-arc basin (i.e., central Italy) where, over a stretched crust, a horst (mainly made up by limestone and Paleozoic metamorphic rocks) and graben (where thick silico-clastic units accumulated) architecture developed.

The structural setting of the study area and its tectonic evolution are characterized by alternating structural highs and lows (narrow elongated basins), with preferential NW–SE and subordinate N–S and E–W alignments.

The interpretation of the available well (Figure 1) and seismic reflection data [e.g., *Buttinelli et al.,* 2014] shows the presence of a massive caprock of about 1800 m of thickness, constituted by the marly calcarenites and clayish marls of the Liguride complex, above a deep reservoir hosting a regional saline aquifer belongs to the Tuscan Nappe.

The stratigraphy of this structure is constrained by well log information of a deep well (Matilde 1, more than 3600 m deep) drilled in 1975 for hydrocarbon exploration and closed soon after because unproductive. The log data were provided by the Vi.D.E.P.I. geodatabase [http://www.videpi.com] of the Italian Ministry of Economic Development (UNMIG) which contains information about public mining permits and concessions archived since 1957.

The stratigraphic setting comprises from bottom to top: Upper Triassic evaporites, Jurassic to Cretaceous, mainly calcareous, successions and Cretaceous-Oligocene flyschoid sediments [*Fazzini et al.*, 1972]. Two major sedimentary cycles close the sequence: the Miocene to Middle Pliocene Lower (with subordinate semi-autochthonous units) and the Middle Pliocene to Quaternary Upper cycles [*Bartole,* 1984, 1990, 1995; *Buttinelli et al.,* 2014].

In addition to the stratigraphy, the data provided by log information of well Matilde 1 (Figure 1), only include measured temperatures, pressure (following the hydrostatic gradient from sea bottom), and salinity (NaCl) of the formation waters collected in carbonate formations (24 g L^{-1}).

3 Reconstruction of mineralogical composition and petrographic analysis

The properties of rocks depend primarily on their mineral composition and microfabric i.e., their structural and textural features [*Rzhevsky and Novik,* 1971]. Consequently, accurate petrographic analyses are a pre-requisite for a correct evaluation of thermal capacity, thermal conductivity, porosity and permeability.

Cuttings and cores of Matilde 1 well are not available. Therefore bulk mineralogical composition was obtained by analysing the inland outcropping samples representative of formations recognized by the well log data (third column in Figure 1). Three areas between Latium and Tuscany Regions (Central Italy) were sampled to obtain analogues of: i) Calcare Massiccio, Calcari Selciferi (c.f. Calcari a Lamellibranchi) and Maiolica (Figure 2; Monte delle Fate); ii) Carbonatic Flysch (c.f. "Flysch della Tolfa"), Arenaceous Flysch (c.f. Pietraforte); Argilloscisti Varicolori (Figure 2; "Cave di Pietra" e Monti della Tolfa); iii) Calcare a Rhaetavicula contorta, Diaspri, Scisti P. (c.f. Scisti Policromi) (Figure 2; Monte Cetona).

The Quaternary Clay, the Rosso Ammonitico and the Anhydriti di Burano formations do not outcrop in the contiguous areas. The mineralogy of Rosso Ammonitico was inferred by the marly facies of Calcare Massiccio [*Morettini et al.,* 2002]. Analysis of Burano were instead carried out on core fragments of the Sabatini 8 well, drilled in-shore for geothermal exploration about 50 km far from Matilde 1. Sabatini 8 cuttings were selected after checking the agreement between Burano core descriptions reported in both well logs. Analysis of Quaternary Clay was performed on core samples kindly provided by Dep. of Science – Roma Tre University.

3.1 Fabric of rock formations

Fabric of representative samples and semi-quantitative analysis of their constituents were determined on polished thin sections integrating polarized light microscopy (Nikon Eclipse E600 Polarizing Microscopy equipped with a Nikon Coolpix 4500 camera; Figure 3).

Fabric classification of clays, claystones and limestones are after *Picard* [1971], *Potter et al.* [1980], *Folk et al.* [1970], *Folk* [1959, 1962], *Dunham [*1962].

Quaternary Clay (c.f. "Argille Azzurre" Fm.)

Quaternary sedimentary rocks are here represented by fine-grained siliciclastic clay-rich mudstones [e.g., *Boggs,* 2009] greyish to green in colour. Considering: the relative low amount of silt-size particles (<35%), with respect to clay-size ones, and the texture described by indurated beds, these rocks could be defined as claystones to silty claystones. Clay minerals are the main constituent, silt-size grains of calcite, quartz and alkali-feldspar are observed.

Carbonatic Flysch (c. f. "*Flysch della Tolfa*"*)*

This flyschoid unit is constituted by calcareous turbiditic sequences characterized by fine granulometry with rare arenaceous strata. Marls and clay layers are present. The base of the sequences is generally characterized by fine detrital limestones and marly limestones. Diagenised layers of carbonatic mudstones are observed. At thin section, the sample is near totally composed by carbonatic (calcite) mud. Rare microcrystals (< 5%) of quartz and clay minerals are observed.

Arenaceous Flysch (c. f. "Pietraforte"Fm.)

This thick arenaceous flyschoid unit is composed of dark grey turbidite sandstones presenting fine to medium particle-size, with subordinate conglomerate beds. Intercalation of laminated clayshales and marls are recognized. Pietraforte, in general, show a major lithic character with abundant carbonatic rocks (> 70%, dolostones, limestones, cherts, claystones and siltstones), and minor metamorphic (10-15%, quartz-phyllades) rock fragments. Cement and matrix are present and are both constituted by calcite and clay minerals. Combining the fine matrix parameter with composition (in QFL model) [after *Williams et al.,* 1982] the Pietraforte sample analysed can be classified as lithic arenite to lithic wacke.

Argilloscisti Varicolori (c.f. Argilloscisti Varicolori Fm.)

A lithologically heterogeneous unit, mainly constituted by gray-to-green laminated claystones with non-regular interbeds of grey carbonatic sandstones, silicic marls and marly limestones. Thin section analyses pointed to a microfabric characterized by a fine carbonatic micritic mudstone presenting rare fine sand, angular to sub-rounded, grains of quartz (≈ 5%) and calcite (≈10%) together with clay minerals (<10%).

Scisti P. (c.f. "Scisti Policromi" Fm.)

This unit is mainly composed by decimetric to metric packed micritic limestone strata, with intercalation of graded calcarenite layers, micritic marls and claystones. Fabric is strongly dependent on granulometry variability, nevertheless it is possible to define this unit as a clay mudstone with rare intercalation of wackestone-packstone. Sparry calcite is not uncommon. Fragments of cherts and limestone are recognized. Analysed sample shows, locally, silicified mudstone textures and presence of clay minerals. Modal composition is here defined: carbonatic material (≈60-65%), quartz (≈30-35%) and clay minerals (<5%).

Maiolica ("Maiolica" Fm.)

Maiolica (Figure 3A) is a pelagic limestone and consists of white calcilutites (with the typical conchoidal fracture) bearing thin layers and nodules of whitish-grey cherts. Minor marls layers and rare black shales beds are also present. In thin section, the sample can be classified as biomicritic-pelmicritic lime-mudstone, with sparry calcite in micrometric veins and replacing microfossils elements. A minor volume of veinlets is sutured by quartz (<5%, on total rock

observed). Stylolites (pressure-solutions structure, suturelike seams with irregular and interlocking penetration of the two sides), characterized by the presence of clay minerals, are observed. Quartz-microveinlets and stylolites are typical structures of Maiolica in the whole Apennine belt.

Diaspri (cf. "Diaspri" Fm.)

This unit is enriched in carbonatic compound and is characterized by rare laminate claymud layers together with chert nodules. Based on thin section observation, the sample is classified as radiolaritic marly mudstone-wackestone with strong heterogeneity in the radiolarian/mud ratio, moreover radiolarian fossils are often substituted by sparry calcite. Modal composition is here defined: carbonatic material (up to 95%) and quartz + clay minerals (≈5%).

Calcari Selciferi (cf. "Calcari a Lamellibranchi") [after *Sturani,* 1967]

Observed samples represent a typical, from hazel-brown to white in colour, mudstone-wackestone (Figure 3B) with dark grey nodular to thin layered jasperoid cherts. Allochem composition is mainly represented by compacted bioclasts and fossils (radiolarians, pelagic lamellibranches, sponge spicules, crinoids and ammonite embryonal shells). Interlayers of lime-mud materials are commonly recognized in respect to clay minerals–rich ones. Sparry calcite – sealed fractures are common for this formation. Considering the jasperoid cherts, the modal composition could be proposed as follow: carbonatic material (≈65%), silica/quartz (≈35%) and clay minerals (< 1%).

Rosso Ammonitico (cf. "Rosso Ammonitico" Fm.)

Rock samples are not available. Description from literature [*ISPRA*, 2007] report minor levels of compacted nodular reddish lime-mud wackestone typified by the presence of ammonites, embryonal ammonite shells and aptychus. Occasionally Rosso Ammonitico shows a bioclastic packstone/grainstone microfabric.

Calcare Massiccio (cf. "Calcare Massiccio" Fm.)

This limestone formation derives by carbonatic organic buildups in a shallow neritic environment [*Wilson*, 1975]. In the study area, Calcare Massiccio is constituted by whitish fossiliferous packstone-grainstone with presence of oncoid and peloid elements. Strata enriched in fossil allochems (Thaumatoporella parvovesiculifera, Paleodasicladus mediterraneus, Solenoporaceae, gastropods, echinoderms and brachiopods) show a boundstone fabric typical of intertidal reef [*Wilson* et al., 1975]. Selected sample in thin section (Figure 3C), shows a nearly total carbonatic composition with very rare quartz grain (≈1%).

Calcare a Rhaetavicula contorta (cf. "Calcari a Rhaetavicula contorta" Fm.)

This unit usually shows a strong vertical variability and lateral facies heteropies. The upper part shows an intraclastic packstone fossil-rich texture with a black to dark greyish colour. Lamellibrach (Rhaetavicula contorta) and bivalve (Megalodon spp., Conchodon spp.) shells represent the major fossiliferous marker. Sparry calcite, together with lime mud, totally fills microfractures and replaces fossil fragments. A lime mud constitutes the matrix. Central portion of the sampled section is a fossiliferous lime-mudstone with intercalation of packstone-grainstone partially recrystallized and dolomitised. Rare vertical unsealed-microfractures are locally reported. Basal portion shows a high grade of dolomitization. Fabric is described by an association of calcareous dolostone and dolomitised saccaroid mudstone with calcite- and

anhydrite- sealed fractures and cavities. Dolomitization, sealed fractures and cavities are typical features of this formation and are interpreted as widespread consequence of late diagenetic process [*Stefani and Trombetta,* 1989]. Analysed thin section (Figure 3D) shows a modal composition described by calcite/dolomite ratio ≈ 3:1 with quartz and clay minerals always minor than 5%.

Burano (cf. "Anidriti di Burano" Fm.)

Burano anhydrites is constituted by an evaporitic succession of anhydrites, dolostones and calcareous dolostones. Anhydrites are variable in colours (white, hazelnut brown, pinkish), well crystallized and locally could contain clay minerals and organic matter. Dolostones (brownish to dark greyish) are ultra-fine saccaroid microcrystalline; while calcareous limestones facies are variable from mudstone to grainstone with a variable allochems (intraclasts, ooids, fossils, and pellets). Polarized light observation of sample selected for thin section indicates anhydrites as major constituent (≈95%) associated with dolomite and calcite elements.

3.2 XRD and calcimetric analyses

Bulk mineralogical compositions were obtained by combining calcimetric determination (carried out with a Dietrich–Fruhling apparatus) and a XRD Rietveld analysis after applying a correction for dolomite to the calcimetry determination.

Clay minerals were determined by XRD on the clay fraction (<2 μm) after reaction with EDTA by analysing oriented-, glycol-, 450 and 600°C treated samples, through the methodology of *Cipriani and Malesani* [1972].

A Rietveld refinement was performed by using the diffraction/reflectivity analysis program Maud 2.2 (Material Analysis Using Diffraction) [*Lutterotti et al.,* 1999] in order to obtain a semi-quantitative analysis. Rietveld quantification procedure permits to calculate the reciprocal ratios among present phases and normalize them (Table 1).

Performed analyses show that the caprock is composed by allochtonous marly calcarenites and clay marls, made up of about 75 and 25% by total volume of carbonates and silicate (quartz, smectite, muscovite, K-feldspar and chlorite) minerals, respectively (Table 1). The reservoir is constituted by pure limestone and marly limestone deposits with calcite and dolomite ranging from 60 to 90% by total volume, respectively, and subordinate quartz and clay minerals (illite, chlorite and Ca-montmorillonite) (Table 1). Triassic evaporites, mainly consisting of anhydrite and dolomite, represent the bottom of the sedimentary sequence.

4 Thermal capacity and thermal conductivity estimation

Thermal capacity and thermal conductivity of rocks was estimated on the basis on mineral assemblage (Table 1).

4.1 Thermal capacity

Thermal capacity of rocks was calculated as a weighted sum from the contributions of the individual mineralogical constituents (Table 1), following the general Kopp's law [e.g., *Rosen and Hashin,* 1970; *Somerton,* 1992; *Clauser,* 2006]:

$$\rho C_{pm} = n_1 C_{m1} C' + n_2 C_{m2} C' + \cdots + n_n C_{mn} C' \quad (1)$$

where ρC_{pm} is the matrix thermal capacity (J m^{-3} K^{-1}), n_n is the fractional volume of mineral n (Table 1), C_{mn} is the molar heat capacity of mineral n (J mol^{-1} K^{-1}) for unit volume at constant pressure and C' is a conversion term (mol m^{-3}) accounting for mineral density and molecular weight. C_{mn} was computed following the equations reported in Table 2.

Thermal capacity increases with the temperature [e.g., *Scharli and Rybach,* 2001]. Its temperature dependence can be empirically calculated by fitting molar heat capacity (C_m) measured at different temperatures directly to polynomials of various degrees [*Maier and Kelley,* 1932; *Haas and Fisher,* 1976; *Berman and Brown,* 1985; *Fei and Saxena,* 1987; *Robertson and Hemingway,* 1995; *Holland and Powell,* 1996].

In this work, polynomial proposed by *Haas and Fisher* [1979] was used for calcite, dolomite, quartz, clays and anhydrite:

$$C_m(T) = K_0 + K_1 T + K_2 T^{-2} + K_3 T^{-0.5} + K_4 T^2 \quad (2)$$

For K-feldspar the *Berman and Brown* [1985] equation was used:

$$C_m(T) = K_0 + K_1 T^{-0.5} + K_2 T^{-2} + K_3 T^{-3} \quad \text{T in Kelvin, (where } K_1, K_2 \leq 0\text{).} \quad (3)$$

Where $C_m(T)$ is in J mol^{-1}K^{-1}, T is temperature in Kelvin and $K_o - K_5$ are the empirical coefficients for polynomials (Table 2).

Temperature correction by polynomial functions is reported working well with error below 10% within a range of 127 – 527°C on various clean to silty sandstones, siltstones, shale, and limestone [e.g., *Somerton*, 1992].

For the purpose of this work molar heat capacity coefficients of smectite as used as proxy of all clay minerals (i.e., montmorillonite, illite and chlorite) since they are characterized by very similar thermo-physical properties.

The thermal capacity of fluids (air, water, gas or oil) occupying pores and fractures of rock plays an important role in the total thermal capacity.

Thermal capacity of water (ρC_{pw}), have be considered in the bulk thermal capacity equation (Kopp's law) in function of porosity, assuming that all pores are filled with water:

$$\rho C_{pb} = \rho C_{pm} \cdot (1 - \varphi) + \rho C_{pw} \cdot \varphi \quad (4)$$

where C_{pb} is the bulk rock thermal capacity (J mol^{-1} K^{-1}), ρC_{pm} is the matrix thermal capacity, ρC_{pw} is the thermal capacity of water, φ is porosity (fraction volume).

On first approximation, not knowing porosity of rocks, an initial theoretic value of 1% was assigned to each formation (third column in Table 3) [*Clauser and Huegens*, 1995; *Singh et al.,* 2007]. This value was successively modified by a trial-and-error procedure to find the best fit with the measured temperature of the well log.

Thermal capacity values for rock samples at in situ formation temperature are reported in Table 3.

4.2 Thermal conductivity

Thermal conductivities of Matilde 1 rock formations were obtained from literature data.

Although thermal conductivity, as thermal capacity, depends on mineralogical composition, microfabric, temperature and saturating fluids [e.g., *Birch and Clark,* 1940; *Brigaud and Vasseur,* 1996; *Clauser and Huenges;* 1996; *Clauser,* 2006], an indirect estimation of this parameter is subject to considerable uncertainties.

This is due to the fact that thermal conductivity of many sedimentary and metamorphic rocks is anisotropic and is controlled not only by mineralogy but also by porosity, size, shape, orientation of pores, density, structure, and fabric of the material as well as degree of crystallization [*Demirci et al.,* 2004; *Gorgulu,* 2004; *Singh et al.*, 2007]. Literature acknowledges for this, and there are many functions that link mineral abundance, volumetric distributions of minerals and thermal conductivity [e.g., *Torquato,* 1991; *Dagan,* 1994]. On the other hand, it is useful to note that a well-connected network of conductive minerals with minor not-conductive minerals have an overall conductivity major than if the contrary happen, for the same mineral composition. Thus the selection of function linking mineral abundances to rock conductivity should be done after a careful investigation of the microstructure of the rocks. Moreover, equations and models for temperature dependence [e.g., *Sass et al.,* 1992; *Funnel et al.,* 1996; *Zoth and Hänel,* 1988; *Seipold,* 1998; *Vosteen and Schellschmidt,* 2003; *Khandelwal,* 2011; *Do and Hoxha,* 2013] introduce further uncertainties, since they can give quite different results for the same rock, even though the thermal conductivity at room temperature are the same [*Lee and Deming*, 1998].

Several extensive compilations of matrix thermal conductivity are available for a large number of rocks [e.g., *Birch,* 1942; *Clark,* 1966; *Desai et al.,* 1974, *Kappelmeyer and Hanel,* 1974; *Roy et al.,* 1981; *Cermak and Rybach,* 1982; *Robertson,* 1988]. These compilations include heterogeneous data, resulting in a great variability of thermal conductivity for each particular rock in function of temperature and anisotropy.

Since the uncertainties in the thermal conductivity estimation, for the purpose of this study thermal conductivities of rocks were computed using the proper equations taken, according to the petrographic investigations, from measured values as function of temperature and pressure listed in *Robertson* [1979, 1988], *Kappelmeyer and Hänel* [1974], *Majzlan et al.* [2002], *Eppelbaum et al.* [2014] directly for the in situ temperatures of Matilde 1 well. For each rock formation, we computed matrix thermal conductivity, taking into account the amount (Table 1) and orientation of minerals such as their thermal conductivities reported in *Diment and Pratt* [1988], *Clauser and Huenges* [1995].

Matrix thermal conductivity values for rock samples (λ_m) at formation temperature are reported in Table 3.

5 Porosity and permeability estimation

Estimated thermal capacity and conductivity of rock formations were successively expressed in function of porosity and permeability by a flow and heat transport modelling. Numerical simulations were carried out simultaneously modifying porosity, permeability and dependent parameters, by a trial-and-error procedure, to find the best fit between calculated and measured well log temperatures, thus obtaining a porosity-permeability profile along the stratigraphic sequence of Matilde 1 well.

The simulations were performed by the Simulator for HEat and MAss Transport (SHEMAT code V.7.1) [*Clauser*, 2003]. SHEMAT solves coupled problems involving fluid

flow, heat transfer, species transport and water-rock interaction [e.g., *Gessner et al.,* 2009; *Kühn,* 2009; *Kühn and Gessner,* 2009a,b] in a wide variety of thermal and hydrogeological problems [e.g., *Kühn et al.,* 2002; 2006; *Kühn and Stöfen,* 2005; *Kühn and Günther,* 2007].

The solution algorithm uses an iterative sequential method to solve for the fluid flow, solute and heat transport. Flow and transport are based on space discretization by finite difference in centred blocks for 2D and 3D Cartesian domains in a saturated porous medium.

The groundwater flow equation used by SHEMAT for variable density conditions is:

$$\rho_f g(\alpha + \varphi\beta)\frac{\partial h_0}{\partial t} = \nabla\left[\frac{\rho_f g k}{\mu}(\nabla h_0 + \rho_m \nabla z)\right] + W' \quad (5)$$

where ρ_f is the fluid density (kg m^{-3}), g is the gravitational acceleration (m s^{-2}), α is the rock compressibility (Pa^{-1}), φ is the porosity, β is the fluid compressibility (Pa^{-1}), h_0 is the hydraulic constant density reference potential (head; m), t is time (s), k is the permeability (m^2), μ is the dynamic viscosity (Pa s), ρ_m is the rock matrix density (kg m^{-3}), z is the elevation (m), W' is the fluid sink or source term (m^3 s^{-1}).

The heat transport equation used by SHEMAT in a Cartesian coordinate system (x, y, z) is :

$$\nabla\left(\lambda\nabla T - \rho_f c_f T\boldsymbol{v}\right) + H = \frac{\partial T}{\partial t}\left(\varphi\rho_f c_f + (1-\varphi)\rho_m c_m\right) \quad (6)$$

where λ is the bulk thermal conductivity (Wm^{-1} K^{-1}), T is the temperature (°C), ρ is the density (kg m^{-3}), c is the specific heat capacity (J k^{-1} kg^{-1}) and the subscripts *f* and *m* signify fluid and rock matrix, respectively; v is the Darcy velocity (m s^{-1}), H is the volumetric heat production (Wm^{-3}); φ is the porosity. Further details on the process capabilities can be found in *Clauser* [2003].

5.1 Model properties

The stratigraphic sequence of Matilde 1 well was reconstructed in SHEMAT by means of a simplified three-dimensional model. The conceptual model has a vertical development of more than 3500 m, from the sea bottom to the basement of the structure, including all the stratigraphic units identified in the well log. Laterally it extends of 1250×1250 m to reduce boundary effects. Maiolica and Diaspri were grouped as an one rock formation since the small tick of Diaspri to reduce the layers number and to favour numerical model convergence. The horizontal domain was discredited using a 8125 cells Cartesian grid, with 25 rows, 25 columns and 13 confined layers.

The system is assumed as a homogeneous porous medium, fully saturated with a NaCl 0.4M (0.24g/L) brine with density of 1005 kg m^{-3}. The limit of this procedure is the assumption that it held only with Darcyan flow. This is true for permeability up to 10^{-12} m^2.

Flow and heat transport are coupled via the dependence of the material and fluid properties on temperature. The Il'in-flux-blending scheme [*Clauser and Kiesner*, 1987] was chosen from options implemented in SHEMAT for solving the equations of heat and species transport. This scheme reduces the numerical dispersion, adapting automatically to the local strength and direction of flow.

The heat transport depends on flow in case of advective heat transfer and by virtue of the pressure dependence of fluid thermal conductivity and fluid volumetric heat capacity. In our model, thermal conductivity and thermal capacity were considered constant at specified in situ temperature, and the coupling of the rock thermal properties on the temperature was disabled.

Matrix thermal conductivity was inserted as input, since SHEMAT internally calculates bulk thermal conductivity (λ) in function of porosity and saturating fluid density according to arithmetic mean:

$$\lambda = \lambda_m \cdot (1 - \varphi) + \lambda_w \cdot \varphi \quad (7)$$

where φ is porosity and λ_m and λ_w are the thermal conductivity (Wm^{-1} K^{-1}) of matrix and water, respectively. Arithmetic mean was preferred to geometric mean for analogy with thermal capacity calculation Eq. (4) and because it is more suitable for samples with conductive matrix.

Initial temperatures of rock formations were assigned by using values measured during the well drilling (Figure 1) and a fixed sea floor temperature of 17 °C [*Bossolasco*, 1954]. Temperature values were permitted to change during the simulation steps.

A constant heat flow of 0.08 W m^{-2}, obtained as results of the calibration procedure, was set as boundary condition at the bottom layer of the model.

No heat or fluid flow across the other boundaries of the domain were allowed. Pore compressibility was set to $1.00\times^{-10}$ Pa^{-1}.

Simulations were performed for a time of 100,000 years in order to achieve the natural state condition.

As mentioned before, an initial porosity of 1% was assigned to all formations. A corresponding initial permeability was estimated among the available and pre-defined porosity-permeability relationships in SHEMAT. Correlation models between porosity and permeability are well established in literature [e.g., *Carman,* 1956; *Verma and Pruess,* 1988] and they depend on the main mineralogical composition of each layer and pore structure. In this study, the fractal ''pigeon hole'' model of *Pape et al.* [1982,1984,1987a,b; 1999] was used since it: *i)* is particularly close to the natural appearance of pore space in sedimentary rocks [e.g., *Kühn et al.,* 2002]; *ii)* accounts for the mineralogical constituents of rock.

A general equation is [*Pape et al.,* 1999]:

$$k = A\varphi^{D_{f1}} + B\varphi^{D_{f2}} + C\varphi^{D_{f3}} \quad (8)$$

where k is the permeability (nm^2), A, B and C are parameters specific for each type of rock, φ is porosity, and the exponent D_{fn} depend on the fractal dimension of the internal surface of the pore space. The coefficients A, B, and C need to be calibrated for each type of rock or chemical pore-space modification.

On the basis of the mineralogical and petrographic analyses (Table 1), we used two relationships accounting for the fraction of clay minerals (i.e., clay coating model) and for the structure of matrix cement minerals (calcite coating and coarse anhydrite models) in the caprock and reservoir, respectively.

The clay coating model combines Eq. (8) with the Kozeny–Carman equation [*Carman,* 1956] which links permeability to the effective pore radius and the formation factor to produce [*Pape et al.,* 1999] a three term power series of porosity:

$$k_{clay} = A\varphi + B\varphi^2 + C(10\varphi)^{10} \quad (9)$$

where A, B and C are parameters derived from a large set of measurements of k and f in the laboratory for different ranges of clay fraction in sandstones (Table 4). The Eq. (9) was applied to the formations constituting the sedimentary coverture above the reservoir and to the Maiolica and Diaspri, since the latter have a limestone fabrics and a matrix particle size characterized by lime-mud (clay-size) biolothitic mudstone (Table 1).

The coating model assumes the presence of small channels whose tortuosity and connectivity depend on the filling material. Therefore the general Eq. (8) reduces to a single exponential term, with different coefficients and fractal exponents for matrix characteristics. For the reservoir, where the matrix cement is mainly calcite, a calcite coating model was applied:

$$k_{calcite} = 42073(10\varphi)^5 \quad (10)$$

For the Burano a coarse anhydrite model was applied:

$$k_{anhydrite} = 0.309(100\varphi)^{4.84} \quad (11)$$

The relationships between porosity and permeability, according to the procedure just described, allow to consider porosity as the one independent variable of model, since thermal capacity and thermal conductivity of rock formations are also expressed as a function of porosity (1%). With a trial-and-error procedure, porosity and the other correlated parameters were simultaneously modified until the best fit between computed and measured temperatures was obtained.

6 Results and discussion

Heat transport simulation results along with the input data are reported in Table 3.

The heat transport simulation in SHEMAT produces as output a temperature value for each cell of the grid model (Figure 4a). Computed temperatures mainly depend on heat flow, porosity and permeability, thermal capacity and thermal conductivity of rock formations. The trial-and-error procedure was performed, changing these parameters, until the obtained temperature profile (Figure 4b) substantially matched the measured temperatures reported in the Matilde 1 well log (Figure 1).

As additional measured temperatures, the AGIP underground data [*AGIP,* 1977], gathering all borehole temperatures achieved during the AGIP research and production of hydrocarbon in Italy, were considered and plotted in Figure 4b. For Matilde 1 well, AGIP book reports temperatures of 30 °C at 297 m b.s.l., 39 °C at 634 m, 88 °C at 2196 m, 86 °C at 2438 m and 115 °C at 3076 m b.s.l..

The goodness of fit between simulated and measured temperatures (including AGIP data) was assessed by the coefficient of efficiency *E* [*Nash and Sutcliffe*, 1970], computed for the same depths interpolating lacking simulated data by a polynomial fitting.

The best fit resulting from the modelled and measured temperature (including AGIP data) shows a coefficient of efficiency E = 0.75. This value is limited by the internal correlation between measured and AGIP data.

Figure 4a shows the computed temperatures in function of depth. Temperatures ranges from 23 °C, at the centroid of Clay, to 144 °C at the centroid of Burano.

Well log measured temperature show wide variations, with a saw tooth shape, especially in the reservoir. The temperature measurements during drilling is a complex function of wellbore geometry, depth, penetration rate, duration of the shut-in intervals, pump and rotary inputs, fluid and formation properties [*Eppelbaum et al.,* 2014]. Then, the measured HT –hole temperatures can significantly differ from the formation equilibrium temperature and should be corrected [*Kutasov and Eppelbaum*, 2015]. Moreover, the determination of transient temperature under circulation and shut-in conditions is complicated by the occurrence of loss circulation [*Fomin et al.,* 2003; 2005; *Bassam et al.,* 2010]. If loss circulation occurs, drilling fluid would be flown into surrounding formation so that it becomes hard to precisely define the temperature profile of a well. In the Matilde 1 well, the temperatures measured at 3132 m and 3492 m b.s.l. (Figure 1) correspond to total loss of circulation. As evidence of the scattering in measured data, the efficiency coefficient between computed temperatures and well log measured values is 0.24, indicating that model prediction is as accurate as the mean of the observed data.

AGIP data has a more linear behaviour with depth, displaying a high coefficient of efficiency with computed temperate (E = 0.99). This good correlation demonstrates that the proposed model is valid and can be considered efficient in the evaluation of the temperature behaviour at depth.

On the basis on both computed temperatures and AGIP data, a geothermal gradient of about 0.0328 °C/m was estimated (first column in Table 3) and plotted in Figure 4b. This substantially follows the temperatures calculated by the heat transport simulation. Small variations between computed temperature and the geothermal gradient are visible in the Calcari a Rhaetavicula contorta and Burano formations, likely due to the presence of convection processes into the most permeable reservoir formations (Figure 4b). If convection is predominant, we would lose the model sensitivity with respect to rock thermal properties, since convection is the most efficient mechanism for heat transfer.

Temperature profile and the heat transport from bottom to surface depend mainly on fluid-dynamic properties of rock formations, i.e. porosity and permeability. In the presented model porosity is a primary variable whereas permeability is related to porosity by *Pape et al.* [1982; 1984; 1987a,b; 1999] correlation model.

The choice of a suitable porosity-permeability relationship is challenging. Because of the complexity and diversity of the pore geometry of natural geologic media, a generally valid porosity-permeability relationship is not always valid for all porous media [*Raffensperger*, 1996], and in some cases different formulations may be preferable [e.g., *Verma and Pruess,* 1988; *Steefel and Lasaga,* 1994] from those applied in this model. This is true especially for carbonatic rocks, cause to their complex faulting and fracture behaviour, the interaction between fractures and matrix rock and the diagenetic processes. The porosity-permeability relationships used in this study are valid for porous media with a fractal behavior such as sandstones. Their

application to carbonatic rocks entails significant uncertainties to model results that are barely quantifiable. However, conventional relationships are weak in carbonates, giving poor results [*Buiting and Clerke,* 2013]. Consequently, the correlation model choice was done according to the petrographic observations and to the most suitable model for such features.

Porosity (Figure 5a) in the caprock is very low, ranging from 3% of flyschoid formations (i.e., Carbonatic and Arenaceous Flysch) and Argilloscisti Varicolori, representing the bottom of Liguride complex, to 5% of Scisti P. that constitute the low permeability top of Tuscan Nappe in this area. Clay at the top of stratigraphic column shows high porosity (i.e. 14%) but low permeability (2.94×10^{-17} m^2; Figure 5b).

The reservoir has higher porosity ranging from 5% of Maiolica and Diapri and Rosso Ammonitico to 9% of Mesozoic limestones (i.e. Calcari Selciferi, Calcare Massiccio and Calcare a Rhaetavicula contorta). The Burano closes the stratigraphic sequence with a porosity of 6%.

Permeability profile varies consequently to porosity, depending from the different applied coating models as function of mineralogical composition (Tables 1 and 3). The Liguride complex shows the lowest permeability (7.65×10^{-18} m^2; Figure 5b), whereas Calcare Massiccio and Calcare a Rhaetavicula contorta have the highest values (2.48×10^{-14} m^2). Although Maiolica and Diaspri belong to the reservoir, they are characterized by a clay-size matrix (i.e., crystal size < 4 μm) that affects the tortuosity of pores. Therefore the use of clay coating model for the layer representing these formations noticeably reduces its permeability (2.04×10^{-17} m^2). Similarly, the significant micritic quartz presence as vein filler in the Calcare Selcifero produces a decreased permeability (i.e., 2.34×10^{-14} m^2) with respect to other carbonatic formations. This decreasing is proportional to the pore space occlusion, reducing the hydraulic section (or increasing tortuosity) due to the vein volume occupied by quartz [e.g., *Nicholl et al.,* 1999]. The Rosso Ammonoitico, characterized by low porosity and permeability values (5% and 1.07×10^{-15} m^2, respectively), constitutes a permeability barrier to fluid and heat transport from bottom to the surface.

Computed permeability values of carbonatic rock formations of reservoir are consistent with values calculated by *Agosta at al.* [2007] for fractured host rocks, belonging to Jurassic-Cretaceous calcareous successions, which range between 7.12×10^{-15} and 6.72×10^{-14} m^2.

Porosity and permeability values of rocks are rarely reported in the well log information. Some values are available in the VIDEPI Project [http://www.videpi.com] for carbonatic formations belonging to Tuscan Nappe since they were among target formations for hydrocarbon explorations. Values reported for limestones widely range from 0.4 to 25% of porosity and from 0.01 to 40 mD (1×10^{-17} to 4.0×10^{-14} m^2), depending on degree of fracturing. Unfortunately these data refer to wells far from the Matilde 1 and they are not properly representative of Matilde 1 diagenesis.

Porosity of Matilde 1 rock formations controls the thermal capacity and the thermal conductivity that were updated for each trial-and-error step. Final values are reported in Table 3 (fourth and fifth column) and showed in Figure 6.

Computed thermal capacity ranges from 2.17 to 2.66 MJ $m^{-3}K^{-1}$ for φ of 1% and from 2.43 to 2.79 MJ $m^{-3}K^{-1}$ in wet conditions. In both cases, highest values are observed for Calcare a Rhaetavicola contorta mainly due to the influence of the dolomite component. The lowest thermal capacity is showed by clays for φ of 1% conditions and by Carbonatic Flysh for wet conditions. In this case a major role is played by the porosity and clay content that control the bulk thermal capacity. Thermal capacity values used in this study result in close agreement with

values reported in *Kappelmeyer and Hänel* [1974]; *Proselkov* [1975]; *Eppelbaum et al*. [2014]; *ETB* [2011] for clays, sandstones, marly and limestones.

Matrix thermal conductivity of Matilde rock formations was obtained from literature data (e.g., compilation data reported in *Eppelbaum et al.* [2014]) for a temperature range of 20 – 200°C, after evaluating the matrix fabric according to the petrographic investigations. Fluid effect was internally computed by SHEMAT on the basis of assigned porosity (Table 3 and Figure 6b). Thermal conductivity at in situ temperature ranges from 1.70 $Wm^{-1}K^{-1}$ of Scisti P. to 4.10 $Wm^{-1}K^{-1}$of Burano. The lowest values were set to Argilloscisti Varicolori and Scisti P., whereas the highest value was set to Burano. In both cases, these values are mainly due to the influence of mineralogical components and temperature. A direct comparison of this study data with other literature values is not easy since the published values of rocks are generally reported at temperature of 25°C. Moreover, temperature dependency functions for thermal conductivity are often not specified.

The proposed method presents many advantages such as the development of an internally consistent dataset and the structured derivation of the main petrophysical reservoir parameters from this dataset.

However, the described approach is prone to some uncertainties, also due to the calibration method of petrophysical data with measured temperatures. The trial-and-error procedure is highly labour-intensive and it requires fundamental knowledge of the model. Moreover, the subjectivity of the manual calibration procedure makes it very likely that many different solutions may lead to equally "good" results [*Boyle et al.,* 2000].

We are aware that a manual calibration can be inefficient for a generally useable method and that an automatic method for parameter optimisation could explore the whole parameter space more efficiently. Although an automatic approach is able to provide objective and good parameter estimates (in the sense that it establishes explicit rules by which the actual sequence of parameter adjustments is made), it can also "degenerate in to pure curve fitting and produce a set of parameters that fit the calibration reasonably well but are hydrologically unrealistic" [Peck, 1976]. To efficiently use automatic methods one should pose constrains to the available range of parameters, thus it also would require a fundamental knowledge of the model.

Finally, the uncertainty in the automatic estimation data diminishes as sample size increases, since the accuracy of any estimator depends on the distribution of the data.

7 Conclusions

A preliminary evaluation of the underground in terms of geological gas storage (CO_2 and /or CH_4) and geothermal energy, also in areas previously unexploited, is becoming an urgent task to reduce anthropogenic emissions of GHG.

An accurate estimate of the underground requires the knowledge of specific parameters compulsory to characterize the thermal and hydraulic properties of the reservoir and to define the reservoir capacity and potentiality.

During the early stage of a feasibility study the availability of data from exploration and development drilling are often lacking and/or inadequate. This work proposed a simple methodology to estimate the rocks petrophysical properties of a selected site integrating mineralogical composition of rock formations, borehole measured temperatures and flow and heat transport modelling. A practical example of this procedure was performed in this work for

an off-shore Italian deep structure reconstructing, from the seafloor to the bottom of the structure, thermal capacity, thermal conductivity, permeability and porosity of rock formations.

The results show a good correlation between the vertical profile of temperature, computed by numerical simulation, and the available borehole temperatures including the AGIP underground data. This supports the validity and reliability of the proposed model, suggesting the possibility of its application in other areas to evaluate their suitability for geological gas storage or geothermal energy application.

Moreover, this simple approach presents many advantages such as the integration of missing data in the porosity, permeability, thermal capacity and conductivity framework through a theoretical approach, providing an internally consistent dataset.

Although the uncertainties of manual calibration, the parameters obtained represent a possible representation of the investigated system and can be an useful tool for both reservoir engineering and geochemical modellers in the assessing of reservoir storage capacity in a first stage of pre-feasibility studies.

Acknowledgments

This research did not receive any specific grant from funding agencies in the public, commercial, or not-for-profit sectors.

The authors wish to thank O. Vaselli and E. Pecchioni for their help during XRD analyses, and M. Procesi and M. Buttinelli for the useful suggestions. Thanks to the Editor and the two anonymous reviewers for their constructive comments on a earlier version of the manuscript.

We note that there are no data sharing issues since all of the numerical information is provided in figures, tables or produced by solving the equations in the paper.

References

Agip (1977), Temperature sotterranee. Inventario dei dati raccolti dall'Agip durante la ricerca e la produzione di idrocarburi in Italia, F.lli Brugoria, Segrate (MI).

Agosta, F., M. Prasad, and A. Aydin, (2007), Physical properties of carbonate fault rocks, Fucino basin (Central Italy): implications for fault seal in platform carbonates, Geofluids 7, 19–32.

Bachu, S., D. Bonijoly, and J. Bradshaw (1977), CO_2 storage capacity estimation: methodology and gaps, Int. J. Greenhouse Gas Control 1 (4), 430–443.

Bartole, R. (1984), Tectonic structures of the Latian–Campanian shelf (Tyrrhenian sea), Boll. Ocean. Teor. Appl. 2, 197–230.

Bartole, R. (1995a), Caratteri sismostratigrafici, strutturali e paleogeografici della piattaforma continentale toscolaziale; suoi rapporti con l'Appennino settentrionale, Boll. So.c Geol. Ital. 109, 599–622.

Bartole, R. (1995b), The North Tyrrhenian–Northern Apennines postcollisional system: constraints for geodynamic model, Terra Nova 7, 7–30.

Bassam, A., E. Santoyo, J. Andaverde, J.A. Hern´andez, and O.M. Espinoza-Ojeda (2010), Estimation of static formation temperatures in geothermal wells by using an artificial neural network approach, Computers and Geosciences 36 (9), 1191– 1199.

Berman, R.G., and T.H. Brown (1985), Heat capacity of minerals in the system Na_2O–K_2O–CaO–MgO–FeO–Fe_2O_3–Al_2O_3–SiO_2– TiO_2–H_2O–CO_2: representation, estimation and high temperature extrapolation, Contrib. Mineral. Petrol. 89, 168–183.

Berryman, J.G. (1995), Mixture Theories for Rock Properties. In: Ahrens T J, editor. Rock Physics & Phase Relations: A Handbook of Physical Constants. Washington, D. C.: American Geophysical Union. doi: 10.1029/RF003p0205.

Birch, F. (1942), Thermal conductivity and diffusivity. In: Birch F, Schairer JF, Spicer HC, editors. Handbook of Physical Constants. New York: Geological Society of America, Special Paper 36, p.243- 266.

Birch, F. (1966), Compressibility; Elastic constant. In: Clark Jr. SP, editor. Handbook of Physical Constants, New York: Geol Soc of America, Memoir 97, 97-173.

Birch, F., and H. Clark (1940), The thermal conductivity of rocks and its dependence upon temperature and composition, Part I,. Am. J. Sci. 238(9), 613-635.

Blondes, M.S., S.T. Brennan, and M.D. Merrill (2013), National assessment of geologic carbon dioxide storage resources– methodology implementation, USGS Open-File Report, p. 26.

Boyle, D.P., H.V. Gupta, S. Sorooshian (2000), Toward improved calibration of hydrologic models: Combining the strengths of manual and automatic methods, Water Resources Research 36 (12), 3663-3674.

Boggs, S.Jr. (2009), Petrology of sedimentary rocks. 2nd ed. Cambridge University Press, p. 607.

Bossolasco, M. (1954), Il regime termico superficiale dei Mari Ligure e Tirreno: I, Geofisica pura e applicata 27(1) , 201-215. doi: 10.1007/bf02033249.

Brigaud, F., and G. Vasseur (1989), Mineralogy, porosity and fluid control on thermal conductivity of sedimentary rocks, Geophysical Journal International 98, 25-542.

Buttinelli, M., D. Scrocca, D. De Rita, and F. Quattrocchi (2014), Modes of stepwise eastward migration of the Northern Tyrrhenian Sea back-arc extension: evidences from the Northern Latium offshore (Italy), Tectonics 33, 187–206.

Buiting, J.J.M. and E.A. Clerke (2013), Permeability from porosimetry measurements: Derivation for a tortuous and fractal tubular bundle, Journal of Petroleum Science and Engineering, 108, 267–278.

Cipriani, C., and P. G. Malsani (1972), Composizione mineralogica delle frazioni pelitiche delle Formazioni del Macigno e Marnoso-arenacea (Appennino settentrionale), Mem. Ist. Geol. e Min. Univ. Padova, 29, 1-25.

Cantucci, B., M. Buttinelli, M. Procesi, A. Sciara, and M. Anselmi (2016), Algorithms for CO_2 storage capacity estimation: Review and case study. In: Vishal V, Singh TN, editors. Geologic Carbon Sequestration. Switzerland: Springer International Publishing Switzerland, p.21-44.

Cantucci, B., G. Montegrossi, M. Buttinelli, O. Vaselli, D. Scrocca, and F. Quatrocchi (2015), Geochemical Barriers in CO_2 Capture and Storage Feasibility Studies, Transp. Porous. Med.106, 107-143. Doi: 10.1007/s11242-014-0392-6.

Carman, P.C. (1956), Flow of Gases Through Porous Media. London: Butterworth Scientific Publications, p.182.

Čermák, V., and L. Rybach (1982), Thermal conductivity and specific heat of minerals and rocks. In: Angenheister G, editor. Landolt-Börnstein: Numerical Data and Functional Relationships in Science and Technology, New Series, V(1a). Berlin: Springer-Verlag, p. 305-343.

Clark, S.P. Jr. (1966), Thermal Conductivity. In: Clark Jr. SP editor. Handbook of Physical Constants. New York: Geol. Soc. of America, Memoir 97, p. 459-482.

Clauser, C. (2003), Numerical Simulation of Reactive Flow in Hot Aquifers - SHEMAT and processing SHEMAT. Heidelberg: Springer Publishers.

Clauser, C. (2006), Geothermal Energy, In: Heinloth K, editor. Landolt-Börnstein, Group VIII: "Advanced Materials and Technologies", Vol. 3 "Energy Technologies", Subvol. C "Renewable Energies", Springer Verlag, Heidelberg-Berlin, p. 480 – 595.

Clauser, C., and E. Huenges (1995), Thermal Conductivity of Rocks and Minerals. In: Ahrens TJ, editor. Rock Physics & Phase Relations: A Handbook of Physical Constants. AGU Ref. Shelf 3.

Clauser, C., and S. Kiesner (1987), A Conservative, Unconditionally Stable, Second- Order Three Point Differencing Scheme for the Diffusion Convection Equation, Geophys, J.R. Astr. Soc. 91 , 557– 568.

Dagan, G. (1994), Significance of heterogeneity of evolving scales to transport in porous formations, Water Resour. Res. 30(12) , 3327-3336.

Demirci, A., K. Gorgulu, and Y.S. Duruturk (2004). Thermal conductivity of rocks and its variation with uniaxial and triaxial stress, Int. J. Rock Mech. Min. Sci. 41, 1133–1138.

Desai, P.D., R.A. Navarro, S.E. Hasan, C.Y. Ho, D.P. Dewitt, and T.R. West (1974), Thermophysical Properties of Selected Rocks. CINDAS Report 23, Center for Information and Numerical Data Analysis and Synthesis (CINDAS), Purdue Univ., West Lafayette, Indiana (USA), p. 256.

Diment, W.H., and H.R. Pratt (1988), Thermal conductivity of some rock forming minerals: a Tabulation. U.S.G.S. Open report 88-690, U. S. Geol. Survey, Denver Co.

Do, D.P., and D. Hoxha (2013), Temperature and Pressure Dependence of the Effective Thermal Conductivity of Geomaterials: Numerical Investigation by the Immersed Interface Method. Journal of Applied Mathematics. http://www.hindawi.com/journals/jam/2013/456931/.

Dunham, R.J. (1962), Classification of carbonate rocks according to depositional texture. In Ham W E, editor. Classification of carbonate rocks, AAPG Memoir 1, 108-121.

Eppelbaum, L., I. Kutasov, and A. Pilchin (2014), Applied Geothermics, Lecture Notes in Earth System Sciences, Springer. DOI: 10.1007/978-3-642-34023-9_2.

ETB (2016), The engineering toolbox. Solids: specific heat capacities, http://www.engineeringtoolbox.com/specific-heat-solids-d_154.html.

Fazzini, P., R. Gelmini, M.P. Mantovani, and M. Pellegrini (1972), Geologia dei Monti della Tolfa (Lazio Settentrionale, provincie di Viterbo e Roma), Memorie della Società Geologica Italiana 11: 65–144.

Fei, Y., and S.K. Saxena (1987), An equation for the heat capacity of solids, Geochim. Cosmochim. Acta 51, 251-254.

Folk, R.L. (1959), Practical petrographic classification of limestones, Am. Assoc. Pet. Geol. Bull.43, 1-38.

Folk, R.L. (1962), Spectral subdivision of limestones types. In Ham, W. E. (ed.), Classification of carbonate rocks, AAPG Memoir 1, 62-84.

Folk, R.L., P.B., Andrews, and D. Lewis (1970), Detrital sedimentary rock classification and nomenclature for use in New Zealand, New Zealand Journal of Geology and Geophysics 13(4), 937-968.

Fomin, S., V. Chugunov, and T. Hashida (2003), Analytical modelling of the formation temperature stabilization during the borehole shut-in period, Geophysical Journal International 155 (2), 469–478.

Fomin, S., T. Hashida, V. Chugunov, and A.V. Kuznetsov (2005), A borehole temperature during drilling in a fractured rock formation, International Journal of Heat and Mass Transfer 48(2), 385–394.

Funnell, R., D. Chapman, R. Allis, and P. Amstrong (1996), Thermal state of the Taranaki Basin, New Zeland, J. Goephys. Res. 101, 25197-25215.

Gailhanou, H., P. Blanc, J. Rogez, G. Mikaelian, H. Kawaji, J. Olives, M. Amouric, R. Denoyel, S. Bourrelly, S. Montouillout, P. Vieillard, C.I. Fialips, N. Michau, and E.C. Gaucher (2012), Thermodynamic properties of illite, smectite and beidellite by calorimetric methods: Enthalpies of formation, heat capacities, entropies and Gibbs free energies of formation, Geochimica et Cosmochimica Acta 89, 279–301.

Gessner, K., M. Kühn, V. Rath, C. Kosack, M. Blumenthal, and C. Clauser (2009), Coupled Process Models as a Tool for Analysing Hydrothermal Systems, Surveys in Geophysics 30, 133-162. doi: 10.1007/s10712-009-9067-1.

Goodman, A., A. Hakala, G. Bromhal, D. Deel, T. Rodosta, S. Fraileyc, M. Small, D. Allene, V. Romanova, J. Fazioa, N. Huertaa, D. McIntyre, B. Kutchkoa, and G. Guthriea (2011), U.S. DOE methodology for development of geologic storage potential for carbon dioxide at national and regional scale, Int. J. Greenhouse Gas Control 5(4), 952–965.

Gorgulu, K. (2004), Determination of relationships between thermal conductivity and material properties of rocks, J. Univ. Sci. Technol. Beijing 11, 297.

Haas, J.L. Jr, and J.R. Fisher (1976), Simultaneous evaluation and correlation of thermodynamic data, Am. J. Sci. 276, 525-545.

Haenel, R., L. Rybach, and L. Stegena (1988), Handbook of Terrestrial HeatFlow Density Determination, Kluwer, Dordrecht, 486 pp.

Hemingway, B.S. (1987), Quartz: Heat capacities from 340 to 1000 K and revised values for the thermodynamic properties, American Mineralogist; 72, 273-279.

Holland, T.J.B. and R. Powell (1996), Thermodynamics of order-disorder in minerals: I. Symmetric formalism applied to minerals of fixed composition, American Mineralogist; 81, 1413-1424.

Jacobs, G.J., D.M. Kerrick, and K.M. Krupka (1981), The High-Temperature Heat Capacity of Natural Calcite (CaCO3), Phys. Chem. Minerals; 7, 55 59.

Kappelmeyer, O., and R. Hanel (1974), Geothermics with Special Reference to Application. Berlin-Stuttgart: Gebtider Bomtrlger, p. 238.

Khandelwal, M. (2011), Prediction of thermal conductivity of rocks by soft computing, Int. J. Earth Sci. (Geol. Rundsch)100, 1383–1389. DOI 10.1007/s00531-010-0550-1.

Krupka, K.M., B.S. Hemingway, R.A. Robie, and D.M. Kerrick (1985), High-temperature heat capacities and derived thermodynamic properties of anthophyllite, diopside, dolomite, enstatite, bronzite, talc, tremolite, and wollastonite, American Mineralogist 70, 261-271.

Kühn, M. (2009), Modelling feed-back of chemical reactions on flow fields in hydrothermal systems, Surveys in Geophysics 30, 233-251. doi: 10.1007/s10712-009-9055-5.

Kühn, M., J. Bartels, and J. Iffland (2002), Predicting reservoir property trends under heat exploitation: interaction between flow, heat transfer, transport, and chemical reactions in a deep aquifer at Stralsund, Germany, Geothermics 31(6), 725-749. doi: 10.1016/S0375-6505(02)00033-0.

Kühn, M., F. Dobert, and K. Gessner (2006), Numerical investigation of the effect of heterogeneous permeability distributions on free convection in the hydrothermal system at Mount Isa, Australia, Earth and Planetary Science Letters 244, 655-671. doi: 10.1016 / j.epsl.2006.02.041.

Kühn, M., and K. Gessner (2009a), Coupled process models of fluid flow and heat transfer in hydrothermal systems in three dimensions, Surveys in Geophysics 30, 193-210. doi: 10.1007/s10712-009-9060-8.

Kühn, M., and K. Gessner, (2009b), Testing hypotheses for the Mount Isa Copper mineralisation with numerical simulations, Surveys in Geophysics 30,253-268. doi:10.1007/s10712-009-9064-4.

Kühn, M., and A. Günther (2007), 4-D hydrothermal reactive transport model based on the regional geological evolution of Allermöhe (Germany), Geofluids 7, 301-312, doi: 10.1111/j.1468-8123.2007.00182.x.

Kühn, M., and H. Stöfen (2005), A reactive flow model of the geothermal reservoir Waiwera, New Zealand, Hydrogeology Journal 13, 606-626. doi: 10.1007/s10040-004-0377-6.

Kutasov, I.M. and L.V. Eppelbaum (2015), Pressure and Temperature Well Testing, CRC Press, Taylor and Francis Inc.

IPCC (2014), Climate Change 2014: Synthesis Report. Contribution of Working Groups I, II and III to the Fifth Assessment Report of the Intergovernmental Panel on Climate Change (Core Writing Team, R.K. Pachauri and L.A. Meyer (eds.)). IPCC, Geneva, Switzerland, 151 pp.

ISPRA (2007), Carta Geologica d'Italia 1:50.000 – Catalogo delle Formazioni (Fascicolo VII), I quaderni del Servizio Geologico d'Italia 7 (VII) - Unità tradizionali (2)/2007.

Lee, Y., and D. Deming (1998), Evaluation of thermal conductivity temperature corrections applied in terrestrial heat flow studies, Journal of Geophysical Research 103 (B2), 2447-2454.

Lutterotti, L., S. Matthies, and H.-R. (1999), MAUD(Material AnalysisUsing Diffraction): a user friendly leakage, therefore a major effort should be done in order to study this kind of systems. Java program for Rietveld Texture Analysis and more, Proceeding of the Twelfth International Conference on Textures of Materials (ICOTOM-12) 1,p. 159.

Maier, C.G., and K.K. Kelly (1932), An equation for the representation of high temperature heat content data, Am. Chemical Soc. J. 54 (8), 3243-3246.

Majzlan, J., A. Navrotsky, and J.M. Neil (2002), Energetics of anhydrite, barite, celestine, and anglesite: A high-temperature and differential scanning calorimetry study, Geochimica et Cosmochimica Acta 66 (10), 1839–1850.

Morettini, E., M. Santantonio, A. Bartolini, F. Cecca, P.O. Baumgartner, and J.C. Hunziker, (2002), Carbon isotope stratigraphy and carbonate production during the Early-Middle Jurassic: examples from the Umbria-Marche-Sabina Apennines (central Italy), Palaeogeography, Palaeoclimatology, Palaeoecology 184, 251–273.

Muffler, L.P.J. (1979), Assessment of geothermal resources of the United States-1978, U.S. Geological Survey Circular 790, p. 163.

Muffler, L.P.J., and R. Cataldi (1978), Methods for regional assessment of geothermal resources, Geothermics 7, 53-89.

Nathenson, M. (1975), Physical factors determining the fraction of stored energy recoverable from hydrothermal convection systems and conduction-dominated areas: U.S. Geological Survey, Open-File Report 75-525, p. 50.

Nash, J. E. and J. V. Sutcliffe (1970), River flow forecasting through conceptual models part I - A discussion of principles, Journal of Hydrology, 10 (3), 282–290.

Nicholl, M.J., H. Rajaram, R.J. Glasss, and R. Detwiler (1999), Saturated flow in a single fracture: evaluation of the Reynolds equation in measured aperture fields, Water resources research 35(11), 3361-3373.

Openshaw, R.E., B.S. Hemingway, R.A. Robie, D.R. Waldbaum, and K.M. Krupka (1976), The heat capacities at low temperatures and entropies at 298.15 K of low albite, analbite, microcline, and high sanidine, J. Res. U.S. Geol. Surv. 4, 195–204.

Pape, H., C. Clauser, and J. Iffland (1999), Permeability prediction based on fractal pore-space geometry, Geophysics 64 (5), 1447–1460.

Pape, H., L. Riepe, and J.R. Schopper (1982), A pigeon-hole model for relating permeability to specific surface, The Log Analyst 23 (1), 5–13. (Errata. The Log Analyst, 23 (2), 50).

Pape, H., L. Riepe, and J.R. Schopper (1984), The role of fractal quantities, as specific surface and tortuosities, for physical properties of porous media, Particle Characterization 1, 66–73.

Pape, H., L. Riepe, and J.R. Schopper (1987a), Theory of self-similar network structures in sedimentary and igneous rocks and their investigation with microscopical methods, J. Microscopy 148, 121–147.

Pape, H., L. Riepe, and J.R. Schopper (1987b), Interlayer conductivity of rocks-a fractal model of interface irregularities for calculating interlayer conductivity of natural porous mineral systems, Colloids and Surfaces 27, 97–122.

Picard, M.D. (1971), Classification of fine-grained sedimentary rocks, J. Sediment. Petrol. 141, 179-195.

Potter, P.E., J.B. Maynard, and W.A. Pryor (1980), Sedimentology of Shale. Springer-Verlag: New York.

Procesi, M., B. Cantucci, M. Buttinelli, G. Armezzani, F. Quattrocchi, and E. Boschi (2013), Strategic use of the underground in an energy mix plan: synergies among CO2,CH4 geological storage and geothermal energy. Latium Region case study (Central Italy), Appl. Energy 110, 104–131.

Proselkov, Y.M. (1975), Heat transfer in wells. Moscow: Nedra (in Russian).

Raffensperger, J.P. (1996), Numerical simulation of sedimentary basin-scale hydrochemical processes. In: Corapcioglu M Y, Editor. Advances in Porous Media, Volume 3. Amsterdam: Elsevier, p.185-305.

Robertson, E.C. (1988), Thermal properties of rocks, Technical report, United States Department of the Interior - U. S. Geological Survey.

Robertson, E.C. (1979), Thermal conductivity of rocks, U.S. Geological Survey Open file report, 79–356.

Robertson, E.C., and B.S. Hemingway (1995), Estimating heat capacity and heat content of rocks, U.S. Open-File Report.

Robie, R.A., S. Russell-Robinson, and B.S. Hemingway (1989), Heat capacities and entropies from 8 to 1000 K of langbeinite ($K_2Mg_2(SO_4)_3$, anhydrite ($CaSO_4$) and of gypsum ($CaSO_4 \cdot 2H_2O$), Thermochimica Acta 139, 67-81.

Rosen, B.W., and Z. Hashin (1970), Effective Thermal Expansion Coefficients and Specific Heat of Composite Materials, International Journal of Engineering 8, 157-173, http://dx.doi.org/10.1016/0020-7225(70)90066-2.

Roy, R.F., A.E. Beck, and Y.S. Touloukian (1981), Thermophysical properties of rocks. In: Touloukian YS, Judd WR, Roy RF, editors. Physical Properties of Rocks and Minerals. McGraw-Hill/ CINDAS Data Series on Material properties, Volume H-2. New York: McGraw- Hill, 409-502.

Rzhevsky, V., and G. Novik (1971), Physical properties of rocks. Moscow: Mir publishers, p. 18.

Sass, J.H., A.H. Lachenbruch, T. Moses, and P. Morgan (1992), Heat flow from a scientific research well at Cajon Pass, California, J. Geophys. Res. 97, 5017–5030.

Schärli, U., and L. Rybach (2001), Determination of specific heat capacity on rock fragment, Geothermics 30(1), 93-110.

Seipold, U. (1998), Temperature dependence of thermal transport properties of crystalline rocks––a general law, Tectonophysics 291,161–171.

Singh, T.N., S. Sinha, and V.K. Singh (2007), Prediction of thermal conductivity of rock through physico-mechanical properties, Building and Environment 42, 146–155.

Somerton, W.H. (1992), Thermal Properties and Temperature Related Behavior of Rock/Fluid, Systems. Amsterdam: Elsevier.

Steefel, C.I., and A.C. Lasaga (1994), A coupled model for transport of multiple chemical species and kinetic precipitation/ dissolution reactions with applications to reactive flow in single phase hydrothermal system, Am. J. Sci. 294, 529–592.

Stefani, M., and G.L. Trombetta (1989). Le successioni Retiche della Toscana orientale e dell'Umbria; cicli sedimentari asimmetrici in un bacino marnoso-calcareo dominato dalle tempeste, Boll. Soc. Geol. It.108(4), 591-606.

Sturani, C. (1967), Réflexions sur les faciès lumachelliques du Dogger Mésogéen (Lumachelle à Posidonia alpina Auctt), Bolletino della Società Geologica Italiana 86, 445-467.

Torquato, S. (1991), Random heterogeneous media : microstructure and improved bounds on effective properties, Appl. Mech. Rev. 44(2), 37-76.

Verma, A., and K. Pruess (1988), Thermohydrological conditions and silica redistribution near high-level nuclear wastes emplaced in saturated geological formations, J. Geophys. Res. 93, 1159–1173.

Vi.D.E.P.I. geodatabase. Ministero dello Sviluppo Economico, Progetto Videpi. http://www.videpi.com

Vosteen, H.-D., and R. Schellschmidt (2003), Influence of temperature on thermal conductivity, thermal capacity and thermal diffusivity for different types of rock, Physics and Chemistry of the Earth 28, 499–509.

Williams, C.F. (2014), Evaluating the Volume Methods in the Assessment of Identified Geothermal Resources, GRC Trans. 38, 967-974.

Williams, H., F.J. Turner, and C.M. Gilbert (1982), Petrography: An introduction to the study of rocks in thin section, WH Freeman and Company.

Wilson, J.L.L. (1975), Carbonate facies in geologic history, Springer-Verlag: New York.

Zoth, G., and R. Hanel (1988), Appendix. In: Haenel R, Rybach L, Stegena L, editors. Handbook of Terrestrial Heat-Flow Density Determination. Kluwer Academic Publishers: Dordrecht.

Table 1. Mineralogical composition of rock formations.

	Sedimentary Coverture					Reservoir					
Formation	Clay	Carbonatic Flysh	Arenaceous Flysh	Argilloscisti Varicolori	Scisti P.	Maiolica & Diaspri	Calcare Selcifero	Rosso Ammonitico[§]	Calcare Massiccio	Calcare a Raetavicola c.	Burano
Mineral	Vol.%	Vol.%	Vol.%	Vol.%	Vol.%	Vol.%	Vol.%	Vol.%	Vol.%	Vol.%	Vol.%
Calcite	25.5	95.20	70.41	83.8	61.20	95.4	66.10	96.10	99.30	74.78	0.20
Quartz	7.0	3.07	15.58	5.36	36.00	3.36	31.40	3.67	0.59	0.60	-
Dol.-dis	1.4	-	1.76	-	-	-	-	-	-	23.98	0.80
K-feldspar	6.2	-	-	-	-	-	-	-	-	-	-
Na-smectite	18.5	-	-	-	-	-	-	-	-	-	-
Illite	4.0	1.3	5.13	3.50	1.10	1.23	0.2	-	-	-	-
Chlorite	6.1	0.12	2.02	3.24	0.21	-	0.2	-	-	-	-
Kaolinite	2.5	-	-	-	-	-	-	-	-	-	-
Muscovite	7.9	-	-	-	-	-	-	-	-	-	-
Ca-Montm.	-	0.28	4.04	4.10	1.40	-	2.0	0.20	-	0.64	-
Anhydrite	-	-	-	-	-	-	-	-	-	-	98.9

Dol.-dis: disordered dolomite. Ca-Mont.: Ca-montmorillonite. [§]: Marly facies of Calcare Massiccio, mineralogical composition was inferred by composition of Calcare Massiccio (Morettini et al., 2002).

Table 2. Equations for mineral molar heat capacity (C_m) calculation in function of temperature.

Mineral	Temperature range (K)	$C_m(T)$ (J mol^{-1} K^{-1})	Reference
Calcite	298-775	$-184.79 + 0.32322T - 3688200\mathrm{T}^{-2} - (1.2974 \times 10^{-4})T^2 + +3883.5T^{-2}$	Jacobs et al., 1995
Dolomite	298-650	$547.88 - 0.16759T + 2.84 \times 10^{6}T^{-2} + 7.7076 \times 10^{-5}T^2$	Krupka et al., 1985
Quartz	298-1000	$81.1447 + 0.0182834T + 5.4058 \times 10^{-6}T^2 - 698.458T^{-0.5} - 180986T^{-2}$	Hemingway, 1987
Clay minerals*	298-1000	$491.66 + 0.74053T + 24000T^{-2}$	Gailhanou et al., 2012
K-feldspar	250-370	$381.37 - 1941T^{-0.5} - 12037300T^{-2} + 1836430000T^{-3}$	Openshaw et al., 1976
Anhydrite	300-1000	$372.80 - 0.1574T + 1695000T^{-2} + 0.00007993T^2 - 4330.8T^{-0.5}$	Robie et al., 1989

T: Temperature (K). * Molar heat capacity coefficients of smectite as used as proxy of all clay minerals.

Table 3. Petrophysical properties of geological formations at in situ temperature, used in the numerical simulations

Formation	T (°C)	ρC_p (T) ($MJm^{-3}K^{-1}$) φ = 1%	ρC_p (T) ($MJm^{-3}K^{-1}$) Final profile	λ_m (T) ($Wm^{-1}K^{-1}$)	φ (%) Final profile	k (m^2) Final profile	φ - k correlation model
Clay	23	2.17	2.43	2.09	14	2.94×10^{-17}	clay coating
Carbonatic Flysh	31	2.31	2.34	2.25	3	7.65×10^{-18}	clay coating
Arenaceous Flysh	62	2.45	2.48	2.56	3	7.65×10^{-18}	clay coating
Argilloscisti V.	95	2.59	2.62	1.71	3	7.65×10^{-18}	clay coating
Scisti P.	98	2.44	2.51	1.70	5	2.04×10^{-17}	clay coating
Maiolica & Diaspri	100	2.48	2.55	2.15	5	2.04×10^{-17}	clay coating
Calcare Selcifero	103	2.46	2.61	2.23	9	2.34×10^{-14}	calcite coating
R. Ammonitico	106	2.59	2.66	2.14	5	1.07×10^{-15}	calcite coating
C. Massiccio	113	2.55	2.69	2.14	9	2.04×10^{-14}	calcite coating
C. Raetavicula	128	2.67	2.80	2.05	9	2.04×10^{-14}	calcite coating
Burano	137	2.60	2.70	4.10	6	1.84×10^{-15}	coarse anhydrite

T: Temperatures in the centroid of each formation following a geothermal gradient of 0.0328 °C/m and a sea temperature of 17°C [*Bossolasco*, 1954], estimated on the basis on both simulated temperatures and AGIP data. $\rho C_p(T)$: bulk thermal capacity at in situ temperature; $\lambda_m(T)$ matrix thermal conductivity at in situ temperature. φ: bulk porosity; k: permeability.

Table 4. Coefficients A, B, C for Eq. (9) for different clay fraction volume

Clay fraction volume	A	B	C
>0.02	31	7463	191
0.02 - 0.10	155	37315	630
0.10 – 0.30	6.2	1493	58
>0.50	0.1	26	1

From *Clauser* (2003).

Captions

Figure 1. Simplified Matilde 1 well-log. Depths (m) are referred to sea level.

Figure 2. Location map of in-shore outcrop rock samples and Matilde 1 well (yellow star). Quaternary clay and Rosso Ammonitico do not outcrop in the contiguous areas. For Burano, cuttings from Sabatini 8 well were used.

Figure 3. Representative Mesozoic limestone fabrics as observed in thin sections at polarized light. **A)** Maiolica mudstone characterized by minor bioclastic elements dispersed in a very fine lime-mud matrix. **B)** Calcari Selciferi mudstone typified by a centimetric jasperoid chert nodule (in dark grey). **C)** Calcare Massiccio biolithitic pakstone-grainstone characterized by the typical biosparitic texture. **D)** Calcare a Rhaetavicula contorta fossiliferous saccaroid packstone.

Figure 4. a) Computed temperature profile vs depth. **b)** Comparison among computed temperatures, well log measured temperatures, AGIP data (*AGIP*, 1977) estimated geothermal gradient for the study area vs depth (m). Depths are referred to sea level.

Figure 5. a) Porosity and **b)** permeability profile vs depth (m) for Matilde 1 well. Depths are referred to sea level.

Figure 6. a) Thermal capacity and **b)** thermal conductivity profiles vs depth (m) for Matilde 1 well. Depths are referred to sea level.

Figure 1.

Matilde 1

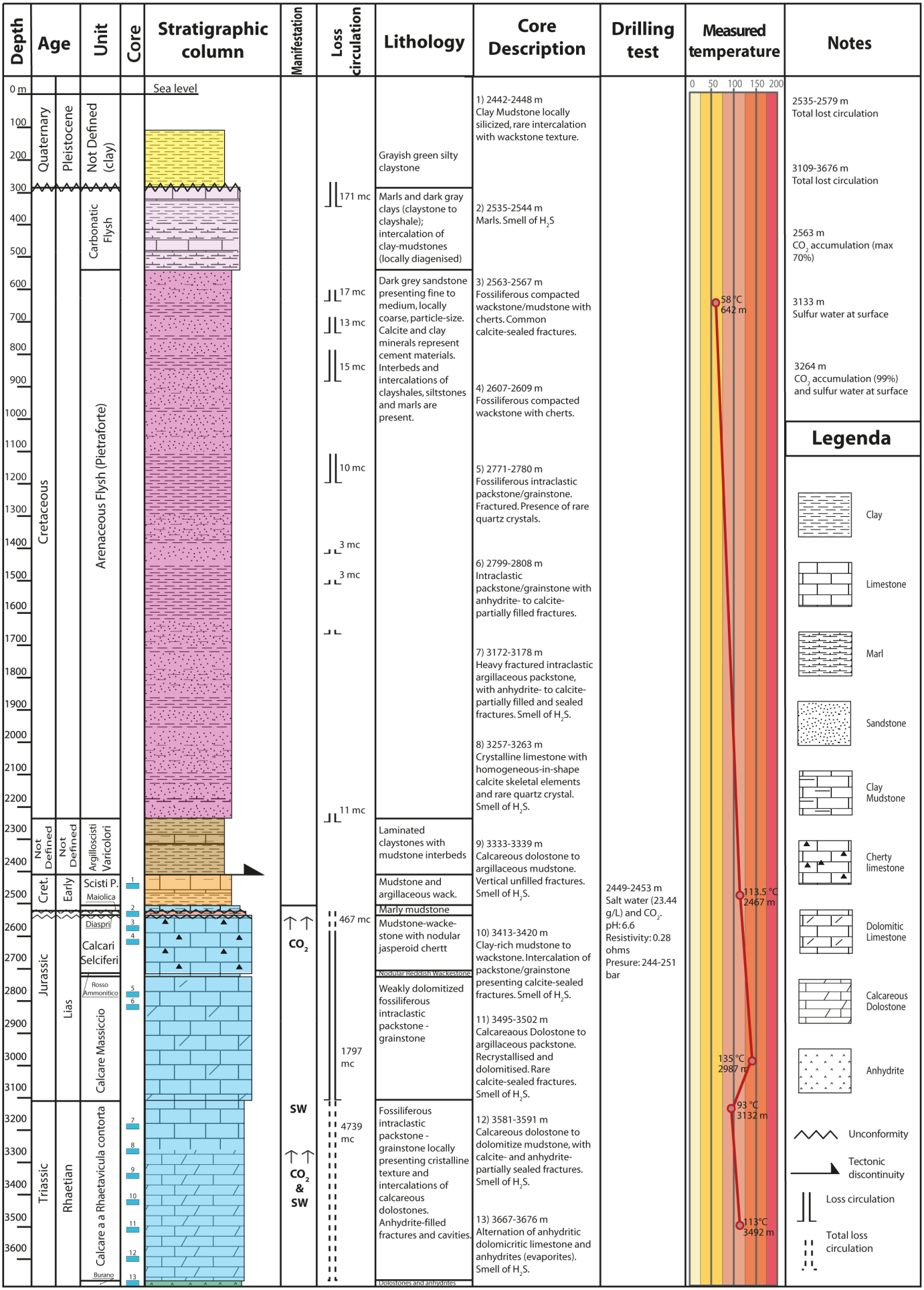

Figure 2.

Locality	Formation
—	Quaternary Clay
●	Carbonatic Flysch
●	Arenaceous Flysch
●	Argilloscisti Varicolori
■	Scisti Policromi
◆	Maiolica
■	Diaspri
◆	Calcari Selciferi
—	Rosso Ammonitico
◆	Calcare Massiccio
■	Calcare a *R. contorta*
◇	Burano

Figure 3.

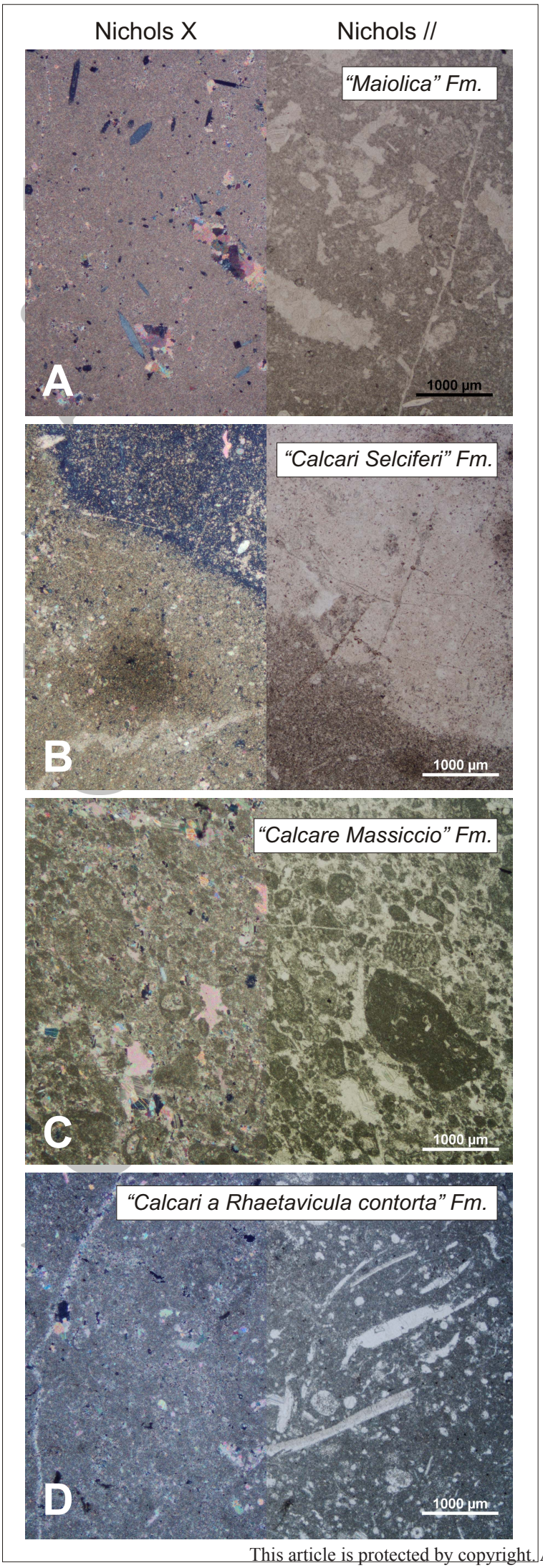

Figure 4.

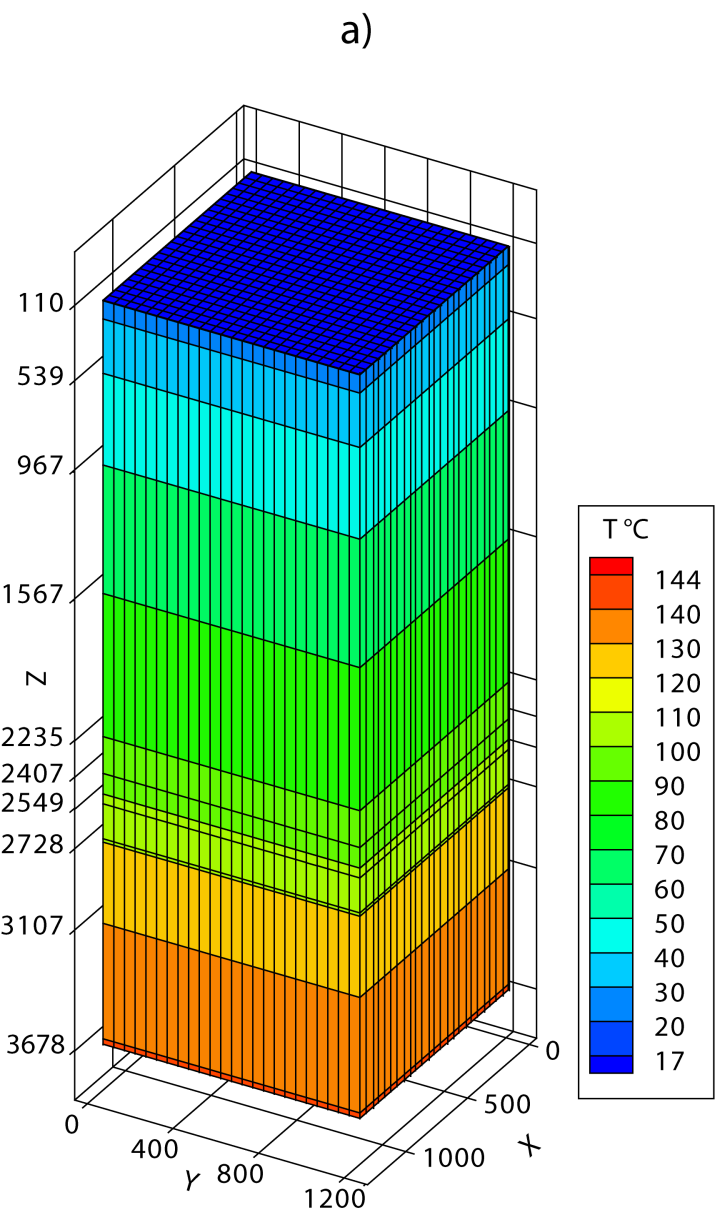

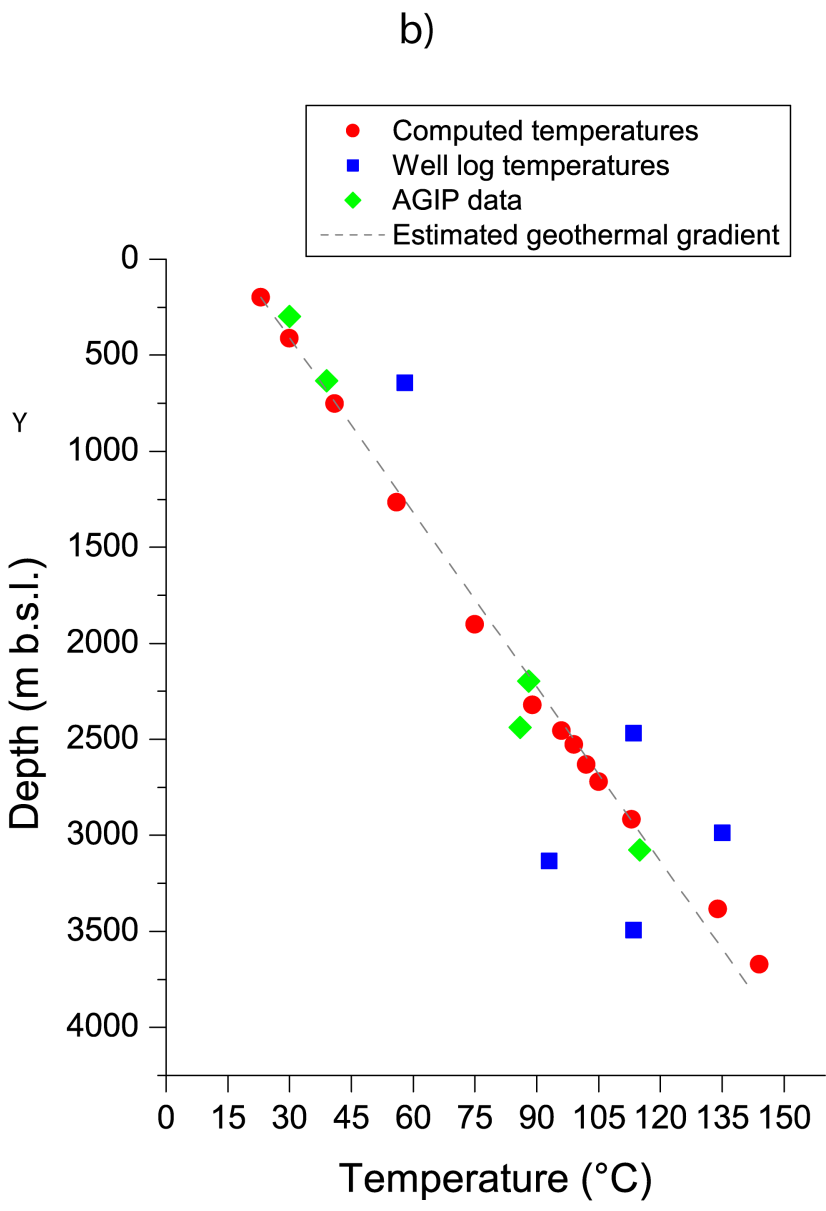

Figure 5.

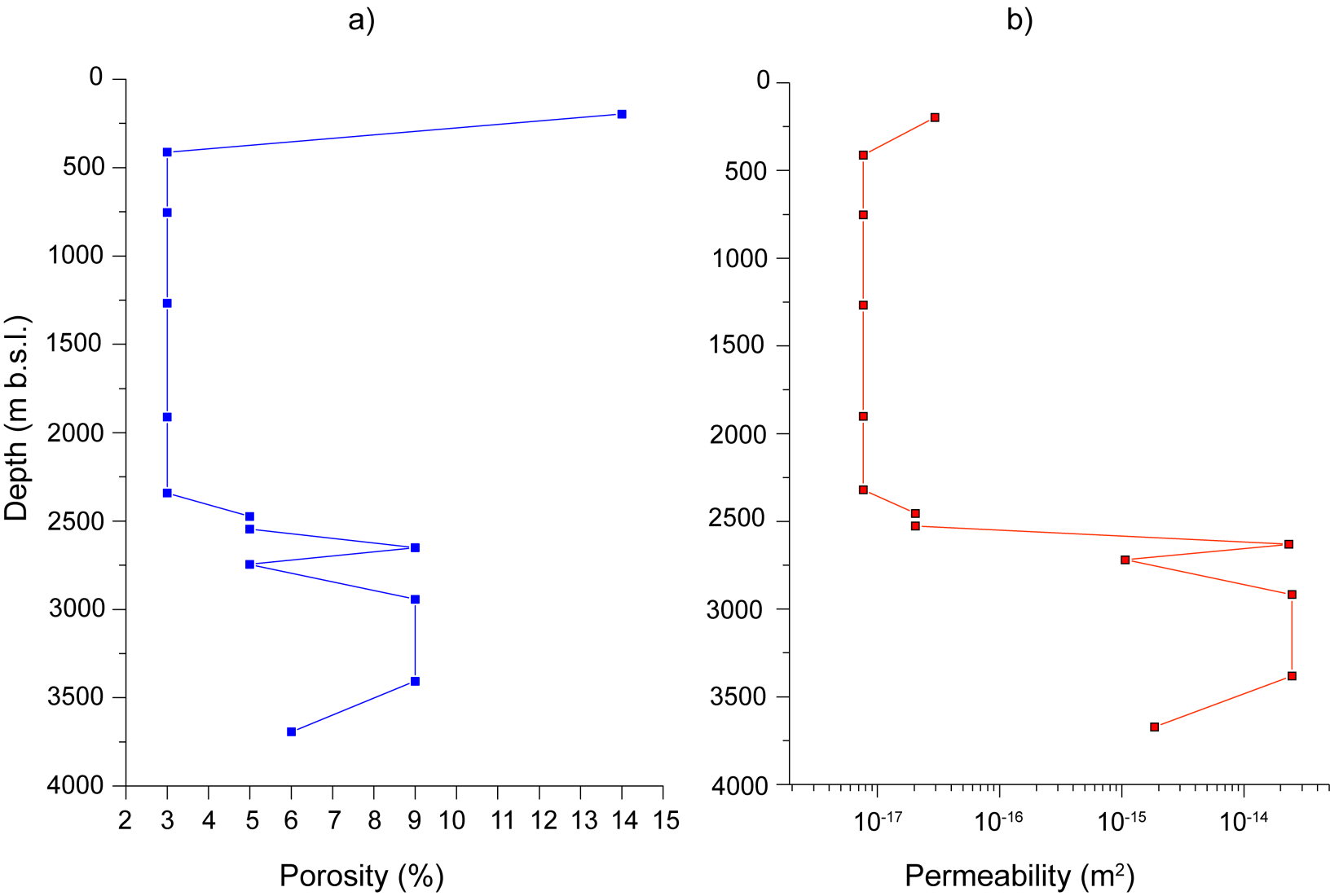

Figure 6.